Nano Research 2014, 7(5): 782–793
DOI 10.1007/s12274-014-0439-6
Research Article
ISSN 1998-0124
CN 11-5974/O4

Unexpected luminescence enhancement of upconverting nanocrystals by cation exchange with well retained small particle size

Mingliang Deng and Leyu Wang (✉)

State Key Laboratory of Chemical Resource Engineering, Beijing Key Laboratory of Environmentally Harmful Chemical Analysis, School of Science, Beijing University of Chemical Technology, Beijing 100029, China

Received: 16 January 2014
Revised: 28 February 2014
Accepted: 02 March 2014

KEYWORDS
cation replacement,
upconversion luminescence,
cell imaging,
luminescence enhancement

ABSTRACT

Highly luminescent upconversion nanoparticles (UCNPs) with small sizes are highly desirable for bioapplications. A facile in situ cation exchange strategy has been developed to greatly enhance the UC luminescence of hexagonal phase $NaYF_4$ NPs while maintaining their small particle size and shape. Via a cation exchange treatment by hot-injecting Gd^{3+} precursors into the as-prepared NPs solution without pre-separation, the naked-eye visible UC emission of the NPs was enhanced about 29 times under 980 nm near infrared (NIR) excitation with unchanged particle size. The cation exchange process was further demonstrated for the case of $NaYF_4$ nanorods (NRs). After the cation exchange, the nanorod was broken into two NPs with stronger emission. The cation exchanged hydrophobic UCNPs were further encapsulated with poly(amino acid) and successfully applied for targeted cancer cell UC luminescence imaging.

1 Introduction

As biomarkers, luminescent nanoparticles (NPs) should be small in size but strong in emission with low autofluorescence [1–6]. However, in general, smaller particle size often results in weaker luminescence owning to the energy loss from nonradiative decay, including vibrational relaxation with the quencher (surface ligands on the nanoparticle surface) and cross-relaxation between the adjacent dopant ions [7]. Due to their low autofluorescence, deep penetration with near-infrared (NIR) irradiation, high photostability, good chemical stability, and low cytotoxicity, rare-earth-doped upconversion (UC) luminescence nanocrystals (NCs) have been widely investigated for sensing and bioimaging [8–25]. Rare earth doped $NaYF_4$ is regarded as one of the most effective UC luminescence matrixes and especially, the luminescence efficiency of $NaYF_4$ with hexagonal phase (β-) is much higher than that of the cubic phase [26–34]. To date, many new methods have been developed to synthesize UC luminescent $NaYF_4$ NCs, such as solvothermal methods [35–39],

Address correspondence to lywang@mail.buct.edu.cn

co-thermolysis methods [1, 40] and microwave-assisted synthesis [41], however, most of the as-prepared small $NaYF_4$ NCs are usually cubic phase with poor UC luminescence [42–44]. Traditionally, to obtain the hexagonal phase $NaYF_4$, the cubic phase precursors were further treated at high temperature, but this leads to larger particle size making the materials unsuitable for bioapplications. Even though some new methods have been developed for the direct synthesis of β-$NaYF_4$ NCs with relatively small size [35, 37, 45, 46], the intensity of their UC luminescence still needs improvement, as the larger specific surface area compared with the bulk material significantly enhances the nonradiative decay on the particle surface. Therefore, it remains a challenge to have small size and strong emission simultaneously in a single nanoparticle.

Coating a homogeneous shell on the surface of NPs has been shown to be an effective way to improve the luminescence performance of small UCNPs [47–54]. The coated shell is believed to increase the distance between the doped ions on the surface of the nanoparticles and the organic surfactant (quencher), which will eliminate the surface defects of the luminescent nanocrystals and enhance the emission efficiency greatly [43, 55]. To carry out the shell coating, however, the obtained nanoparticle seeds need to be treated through washing, drying, dissolving in organic solvents, and then coating [56], which is time-consuming and sometimes leads to aggregation of NPs. Furthermore, the shell coating usually results in enlargement of the particle size. Another method to fabricate the core-shell semiconductor NPs is cation exchange [57, 58]. In order to introduce the T_1-imaging functionality for magnetic resonance imaging (MRI), the hydrophobic $NaYF_4$ NPs (~20 nm) have been transferred into aqueous solution by coating with polyvinylpyrrolidone (PVP) and then the $NaGdF_4$ shell was formed on the surface of $NaYF_4$:Yb/Tm@PVP NPs via cation exchange. But the luminescence of these core–shell NPs is enhanced only about 0.38 times compared with the NPs without the $NaGdF_4$ coating [59]. Up to now, there has been no report of a way to greatly enhance the upconversion luminescence of $NaYF_4$:Yb^{3+}/Er^{3+} NPs via one-pot *in situ* cation exchange while maintaining the small particle size.

Herein, we present a facile *in situ* one-pot Gd^{3+}-exchange strategy to enhance the UC luminescence of $NaYF_4$:Yb^{3+}/Er^{3+} NPs about 29 times with unchanged particle size (~11.8 nm). The Gd^{3+}-exchange was carried out after the formation of $NaYF_4$:Yb^{3+}/Er^{3+} NPs independent of separation and surface modification. In the case of $NaYF_4$: Yb^{3+}/Er^{3+} nanorods (NRs), after the exchange with Gd^{3+}, the nanorod was broken into two NPs with stronger emission. To demonstrate their bioapplications, the hydrophobic Gd^{3+}-exchanged $NaYF_4$: Yb^{3+}/Er^{3+} UCNPs were functionalized with poly(amino acid) and successfully applied for targeted cell imaging.

2 Experimental

2.1 Chemicals and reagents

All lanthanides were obtained from Beijing Ouhe Chemical Reagent Co. Oleylamine, dimethylsulfoxide (DMSO), oleic acid, sodium stearate, 1-octadecene, hydrofluoric acid, ethyl dimethylaminopropyl carbodiimide solution (EDC), *N*-Hydroxysuccinimide (NHS), and methyl thiazolyl tetrazolium (MTT) were purchased from Sigma-Aldrich. The polysuccinimide (PSI) was obtained from Shijiazhuang Desai Chemical Company. Ethanol, sodium hydroxide, *N*, *N*-dimethylformamide (DMF), and cyclohexane were supplied by Beijing Chemical Reagent Co. All cell culture reagents were supplied by M&C Gene Technology (Beijing) Ltd. All chemicals were analytical grade and used directly without further purification. Deionized (DI) water was used throughout.

2.2 Characterization

Powder X-ray diffraction (XRD) patterns of the NCs were recorded on an Ultima III X-ray powder diffractometer (Rigaku, Japan) with Cu Kα radiation of wavelength λ = 1.5418 Å. The size and morphology of the NCs were examined with a Supra 55 scanning electron microscope (SEM) (Zeiss, Germany), JEM-1200EX transmission electron microscope (TEM) (JEOL, Japan) and JEM-2100F high-resolution transmission electron microscope (HRTEM) (JEOL, Japan). High angle annular dark field scanning transmission electron microscopy (HAADF-STEM) images and corresponding elemental mappings were examined

with a Tecnai F20 field emission gun transmission electron microscope (FEI, America). Energy dispersive X-ray (EDX) analysis was recorded on Supra 55 scanning electron microscope (Zeiss, Germany). Inductively coupled plasma mass spectrometry (ICP-MS) (7700 ICP-MS, Agilent, America) was employed to detect the concentration of Gd^{3+} doped in the NCs. The relaxivity (r_1) was characterized at 298 K by an Avance DPX-400 nuclear magnetic resonance (NMR) spectrometer (Bruker, Germany). The luminescence properties were measured on an F-4600 spectrophotometer (Hitachi, Japan) equipped a 980–nm NIR diode laser. The *in vitro* cell viability was tested by a Tecan Infinite F50 (Switzerland) plate reader. Cell imaging was recorded with a TCS SP5 two-photon confocal microscope (Leica).

2.3 Synthesis of the $NaYF_4$ NPs and NRs

The precursors of Gd^{3+}–oleate and $Y^{3+}/Yb^{3+}/Er^{3+}/Tm^{3+}$ mixed oleate were synthesized through our previously reported method with a minor alteration [22]. In brief, 0.36 g of sodium hydroxide, 3 mL of oleic acid, 4 mL of ethanol, 6 mL of deionized (DI) water, and 15 mL of cyclohexane were added to a 50-mL Teflon-lined autoclave under stirring. Then 10 mL of lanthanide nitrate (Y^{3+}, Yb^{3+}, Er^{3+}, Tm^{3+}, or Gd^{3+}) aqueous solution (0.5 M) was added into the mixture which was stirred for another 10 min. The autoclave was then sealed and heated at 80 ℃ for 4 h before it was allowed to cool naturally to room temperature. Thereafter, the colloid of rare earth oleate in the oil layer was gathered and diluted to 20 mL with cyclohexane. The relative ratio of Y^{3+}, Yb^{3+}, Er^{3+}, and Tm^{3+} to total rare earth amount was changed as desired to investigate the influence on the UC emission color, respectively. Transparent $R–NH_3^+F^-$ (R is the long alkyl chain of oleylamine, C_{18}) was prepared by adding 3 mL of HF, 17 mL of oleylamine, 3 mL of cyclohexane and 7 mL of ethanol. $R–NH_3^+F^-$ is an involatile ammonium salt and thus the corrosivity to the glass and consequently the toxicity of original HF were greatly reduced.

The luminescent β-$NaYF_4$:$Yb^{3+}/Er^{3+}/Tm^{3+}$ NPs were synthesized as follows. In brief, a three-necked flask containing 7 mL of oleic acid, 8 mL of octadecene, and 0.35 g of sodium stearate was heated to 80 ℃ under stirring. Then 4 mL of the rare earth oleate solution (1.0 mmol) and 1.4 mL of $R\text{-}NH_3^+F^-$ solution were injected into the flask orderly before the mixture solution was treated at 80 ℃ for 20 min. The solution was then heated to 180 ℃ and kept at this temperature for 10 minutes. The $NaYF_4$:Yb/Er/Tm NPs were prepared after the solution was treated at 310 ℃ for different time (0–60 min). Then the solution was cooled down to room temperature and the product was centrifuged and washed three times with ethanol and cyclohexane. The final UCNPs were collected and dispersed into 5 mL of cyclohexane. The synthetic procedures for $NaYF_4$ NRs were similar to that of the $NaYF_4$ NPs with minor alteration. Briefly, 15 mL of the oleic acid without octadecene was added into a flask and the solution was treated at 310 ℃ for 1 h.

2.4 Synthesis of Gd^{3+}-exchanged β-$NaYF_4$ NCs

The pure Gd^{3+}–oleate precursor was first heated at 80 ℃ for about 15 min to remove the low-boiling-point small molecules completely and turn the precursor into the glue. After cooling down to room temperature, the solid precursor was stored at 4 ℃ for later use. The $NaYF_4$:Yb^{3+}/Er^{3+} NCs with controllable sizes and morphology were prepared according to the aforementioned method. As the reaction solution containing the $NaYF_4$:Yb^{3+}/Er^{3+} NCs was heated at 310 ℃ for 0.5 h, desired amount of Gd^{3+}-oleate precursors were added into the flask directly and the reaction was held for another 0.5 h at this temperature under stirring. Finally, the reaction solution was cooled down to room temperature and the product of Gd^{3+}–exchanged β-$NaYF_4$:Yb^{3+}/Er^{3+} NCs was collected by centrifugation three times with ethanol and cyclohexane.

2.5 Surface modification of Gd^{3+}–exchanged UCNPs

Before the surface modification of the hydrophobic NPs, the polysuccinimide, a poly(amino acid), was first modified with oleylamine as follows [60, 61]. Briefly, oleylamine (1.2 mL) was first mixed with DMF (30 mL) containing PSI (1.2 g), and the mixture was then treated at 100 ℃ for 5 h. After cooling to room temperature, the solution was precipitated and washed with methanol. After evaporating the residual methanol, the oleylamine-modified polysuccinimide (oleylamine–PSI) was redispersed into chloroform. To functionalize the hydrophobic luminescent UCNPs, 1.0 mL of

chloroform containing Gd^{3+}–exchanged $NaYF_4$:Yb^{3+}/Er^{3+} NPs (3.8 mg) and oleylamine–PSI (28 mg) were added into 10 mL of NaOH (5.0 mM) aqueous solution under ultrasonication. After evaporating the chloroform, the poly(amino acid) coated nanocrystals were collected by centrifugation and redispersed into 2.0 mL of deionized water.

2.6 Cytotoxicity tests

To evaluate the cytotoxicity of the Gd^{3+}–exchanged $NaYF_4$:Yb^{3+}/Er^{3+} NPs, about 5×10^4/well hepatocellular carcinoma cells (HepG2) were seeded into a 96-well cell culture plate and cultured overnight at 37 ℃ under 5% CO_2. Then different amounts of the poly(amino acid) functionalized UCNPs (0–200 μg/mL) were added into the plate and cultured with the HepG2 cells for 24 and 48 h, respectively. Thereafter, 20 μL of methyl thiazolyl tetrazolium (MTT, 5 mg/mL) was added into each well and incubated for another 4 h. Solid product, formazan, deposited in the bottom of well was then dissolved by adding 150 μL of DMSO. The absorbance of dissolved formazan at 490 nm is dependent upon the degree of activation of the cells and was detected.

2.7 Bioconjugation of anti-α-fetoprotein (anti-AFP) antibody (Ab) with UCNPs

In brief, 100 μg of the oleylamine–PSI modified Gd^{3+}–exchanged $NaYF_4$:Yb^{3+}/Er^{3+} luminescent UCNPs, 20 μL of ethyl dimethylaminopropyl carbodiimide solution (EDC, 10 mg/mL) and 20 μL of N-hydroxysuccinimide (NHS, 25 mg/mL) were mixed together and incubated in a reciprocating oscillator at 25 ℃ for 30 min to activate the carboxyl groups on the UCNPs. 10 μL of anti-AFP antibody (1 mg/mL) was then added into the mixture and kept incubation for another 2 h at 25 ℃. The mixture was then incubated with 20 μL of bovine albumin (BSA, 50 mg/mL) to deplete the excess carboxyl groups. Finally, the UCNPs–Ab (anti-AFP) NPs were collected by centrifugation for two cycles (10,000 rpm, 10 min) and redispersed in PBS (pH = 7.4, 100 μL).

2.8 UC luminescence imaging of cancer cells with UCNPs–Ab (anti-AFP)

HepG2 or HeLa cells were seeded on a clean cover slide and cultured in 6-well cell culture plate overnight. Then the cells were stained with 100 μg/mL of UCNPs–Ab (anti-AFP) under 5% CO_2 at 37 ℃ for 4 h. Cell imaging was then carried out under 980 nm NIR excitation after washing the cells with PBS three times to remove the free UCNPs–Ab and fastening the cells by 4% paraformaldehyde solution. To confirm the specific recognition between the Ab (anti-AFP) and the HepG2 cancer cell, the UCNPs and UCNPs–Ab were incubated with HepG2 cell and HeLa cells, respectively.

3 Results and discussion

The $NaYF_4$ UCNPs precursors and Gd^{3+}-exchanged UCNPs were synthesized under N_2 atmosphere. To investigate the effects of Gd^{3+}-exchange on the luminescence enhancement and particle size of UCNPs, the green emission of $NaYF_4$ (Y^{3+}/Yb^{3+}/Er^{3+} = 80/15/5) NPs with small sizes were used as the seeds for the preparation of Gd^{3+}-exchanged UCNPs. The reaction solution containing the as-prepared $NaYF_4$: Yb^{3+}/Er^{3+} NPs was further treated with Gd^{3+}–oleate at 310 ℃ for another 30 min to obtain the Gd^{3+}-exchanged UCNPs. The effects of Gd^{3+}–oleate dosage on the size and luminescence of UCNPs were investigated in detail (Figs. 1(a1)–1(e1)). As a control, the bare $NaYF_4$: Yb^{3+}/Er^{3+} NRs without Gd^{3+}–exchange were also prepared (Fig. 1(f1)). The corresponding UC luminescence spectra and photos of the bare $NaYF_4$:Yb^{3+}/Er^{3+} NPs without Gd^{3+}–exchange (Figs. 1(a2) and 1(a3)), Gd^{3+}-exchanged $NaYF_4$: Yb^{3+}/Er^{3+} NPs with different dose of Gd^{3+}–oleate (Figs. 1(b)−1(e)) and bare $NaYF_4$: Yb^{3+}/Er^{3+} NRs (Figs. 1(f2) and 1(f3)) are also shown. It is well known that the luminescence of nanoparticles is easily quenched by organic chemicals (or water) with high vibrational energy on the particle surface [53, 62]. Hence, the decrease in nanocrystal size will lead to a marked increase of the specific surface area and thus obvious luminescence quenching. Due to the large particle size (46/26 nm), the UC emission of bare $NaYF_4$:Yb^{3+}/Er^{3+} NRs without Gd^{3+}–exchange (Fig. 1(f)) is about 2.8 times as strong as that of bare $NaYF_4$:Yb^{3+}/Er^{3+} NPs (Fig. 1(a)) whereas the total treatment time at 310 ℃ is identical (1 h) for each sample. The green UC emission of the Gd^{3+}-exchanged

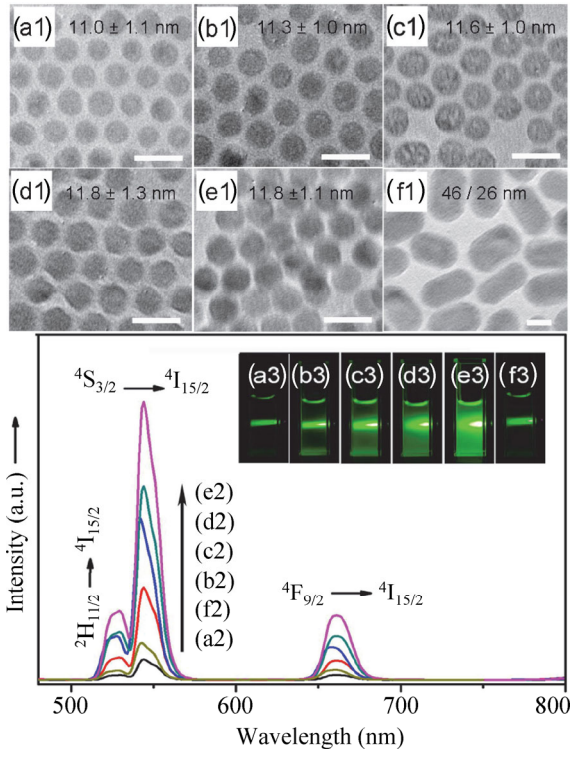

Figure 1 TEM images and UC luminescence spectra and photographs of $NaYF_4$:Yb^{3+}/Er^{3+} NPs (a)–(e) and NRs (f). Dosage of Gd^{3+}: (a1)–(a3) 0, (b1)–(b3) 0.25, (c1)–(c3) 0.5, (d1)–(d3) 0.75, (e1)–(e3) 1.0, and (f1)–(f3) 0 mmol in the as-prepared β-$NaYF_4$:Yb, Er NCs solution (containing 1.0 mmol of rare earth ions). Total reaction time is 1.0 h at 310 ˚C for each sample. Scale bars are 20 nm. Nanomaterials were excited via a 980-nm diode laser with an irradiation power of 0.4 W. The photographs (insert) were taken by dispersing nanocrystals in cyclohexane with the concentration of 0.2 M.

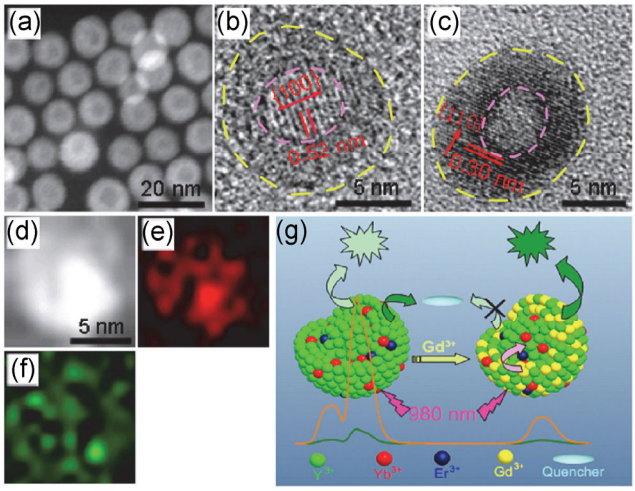

Figure 2 (a) STEM image, (b) and (c) HRTEM images, (d)–(f) Single nanoparticle HAADF-STEM image and corresponding elemental maps [Y ((e) red) and Gd ((f) green)] of Gd^{3+}-exchanged $NaYF_4$ NPs encapsulated with poly(amino acid). (g) Schematic illustration of enhanced emission of Gd^{3+}-exchange on the UCNPs.

$NaYF_4$:Yb^{3+}/Er^{3+} NPs (0.5 mmol Gd^{3+}, Fig. 1(c)) is far stronger (~13 times) than that of bare $NaYF_4$:Yb^{3+}/Er^{3+} NPs and ~4.8 times as strong as that of bare $NaYF_4$:Yb^{3+}/Er^{3+} NRs, but their sizes have no significant difference. As the Gd^{3+} dose was increased to 1.0 mmol (Fig. 1(e)), the green UC emission enhanced about 29 times compared to that of bare UCNPs. The obvious UC emission enhancement can be attributed to the inert Gd^{3+}-exchanged shell with low phonon energy that promoted the energy transfer from Gd^{3+} to the activator (Yb^{3+}). Meanwhile, as shown in Fig. 2(g), the quencher was separated in space by the inert Gd^{3+}-exchanged shell from the emission centers [47]. Hence, the inert shell also greatly reduced the vibrational relaxation between luminescent ions and the organic surfactant and eliminated the surface defects of the luminescent nanocrystals. Different from the reported shell coating strategy for core–shell NPs, these Gd^{3+}-exchanged $NaYF_4$:Yb^{3+}/Er^{3+} NPs showed no obvious change in the particle size and shape. These results suggest that it is feasible to get stronger emission whilst retaining small particle size—which is highly desirable for biomedical imaging applications—via this facile strategy.

In order to confirm that the UC luminescence enhancement results from the Gd^{3+}–exchange rather than a crystal phase transition, the crystal structures of the as-synthesized UCNPs before and after Gd^{3+}-exchange were characterized by powder XRD. The position of the diffraction peaks is consistent with that of the reference hexagonal phase $NaYF_4$ (Fig. S1 in the Electronic Supplementary Material (ESM), JCPDS card No. 16-0334). It is noteworthy that the Gd^{3+}-exchange has no effect on the crystal structure of β-$NaYF_4$ UCNPs. Meanwhile, the energy dispersive spectrometry (EDS) analysis (Fig. S2 in the ESM), elemental analysis by ICP-MS assay and the magnetic resonance (MR) relaxivity (T_1) measurements (Fig. S3 in the ESM) confirmed the presence of Gd^{3+} ions in the exchanged UCNPs. Therefore, the UC luminescence enhancement results from the Gd^{3+}–exchange rather than a phase transition of the UCNPs.

To further characterize the Gd^{3+}-exchange in the

UCNPs, HRTEM (Figs. 2(b) and 2(c)), STEM (Figs. 2(a) and 2(d)) and corresponding elemental mapping analysis (Figs. 2(e) and 2(f)) of the Gd^{3+}-exchanged $NaYF_4$ NPs were recorded. The HRTEM images in Figs. 2(b) and 2(c) revealed that the $NaYF_4$ NPs, with the lattice distance of 0.52 nm corresponding to the {100} planes, were corroded by Gd^{3+}, and the core size was about 5.0 nm. The elemental mapping of HAADF-STEM micrograph showed that Y and Gd were mainly distributed in the center and edge of the nanocrystals, respectively (Figs. 2(e) and 2(f)).

Electron beam damage at high magnification may cause NPs to become hollow and take on core–shell morphologies [63], and in order to eliminate this possibility, we also analyzed the TEM data of Yb–Er–Gd co-doped $NaYF_4$ NPs ($Y^{3+}/Yb^{3+}/Er^{3+}/Gd^{3+}$ = 64/12/4/20) at the same magnification and no core-shell morphologies was observed (Fig. 3(b)). Unlike the Gd^{3+}-exchange UCNPs, the elemental mapping of the HAADF-STEM micrograph showed that both Y and Gd were distributed uniformly in the nanocrystals (Fig. 3(c)). The luminescent properties of these $NaYF_4$:Yb/Er/Gd NPs were also investigated. As shown in Fig. 3(d), the UC luminescence efficiency of the $NaYF_4$:$Yb^{3+}/Er^{3+}/Gd^{3+}$ NPs was even lower than that of untreated $NaYF_4$:Yb^{3+}/Er^{3+} NPs. These results further suggest that the luminescence enhancement of Gd^{3+}-exchanged $NaYF_4$ NPs is attributed to the successful Gd^{3+}-exchange but not Ostwald ripening.

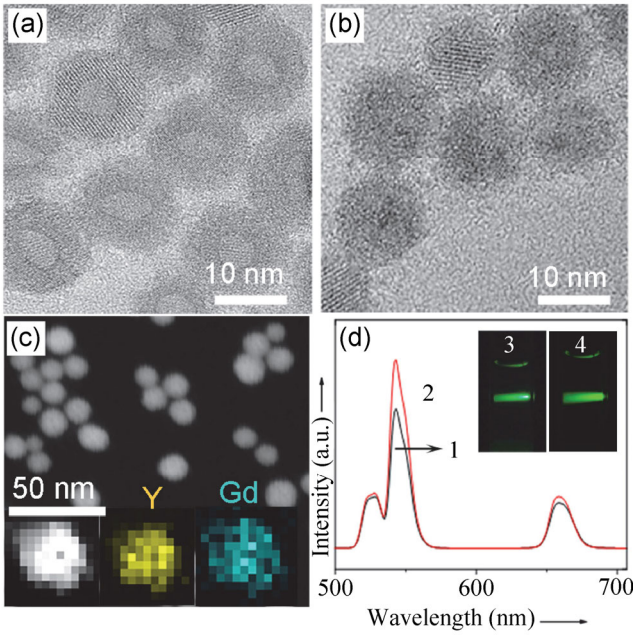

Figure 3 (a) Large area HRTEM image of Gd^{3+}-exchanged $NaYF_4$:Yb^{3+}/Er^{3+} NPs. (b) HRTEM and (c) STEM image and corresponding elemental maps [Y (yellow) and Gd (blue)] of the Yb–Er–Gd co-doped $NaYF_4$ NPs, and the UC luminescence spectra (d) and photographs (insert) of Yb–Er–Gd co-doped $NaYF_4$ NPs (1, 3) and the untreated $NaYF_4$:Yb^{3+}/Er^{3+} NPs (2, 4).

As aforementioned, the green UC luminescence efficiency of hexagonal phase $NaYF_4$ is much higher than that of the cubic phase one [22, 27, 64]. In order to obtain hexagonal phase $NaYF_4$:Yb^{3+}/Er^{3+} UCNPs with small particle sizes, we first investigated the influence of reaction time on the crystallization and sizes of the UCNPs in detail before the Gd^{3+}-exchange. The UCNPs treated at 310 ℃ for different times were characterized by TEM (Figs. 4(a)–4(f)) and powder XRD (Fig. 4(g)). Originally, the ultra-small $NaYF_4$:Yb^{3+}/Er^{3+} seeds (~2.3 nm, UCNPs precursors) obtained by mixing the rare earth oleates and HF–oleylamine and treating at 180 ℃ were cubic phase (Fig. 4(a)). After the UCNPs precursors were treated at 310 ℃ for 5 min, ultra-small cubic phase $NaYF_4$:Yb^{3+}/Er^{3+} NPs with a size of ~4.6 nm were obtained (Fig. 4(b)). As the reaction time was extended to 9 min, both cubic and hexagonal phases $NaYF_4$:Yb^{3+}/Er^{3+} NPs (~6.5 nm) with irregular shape were found (Fig. 4(c)). Even when the reaction time was prolonged to 15 min (Fig. 4(d)), some cubic phase UCNPs were still found in the final products. Meanwhile, most of the UCNPs were ~8.9 nm in size, but many small particles surrounding the large particles were observed. When the precursors were treated at 310 ℃ for 30 or 60 min, uniform and pure hexagonal phase $NaYF_4$:Yb^{3+}/Er^{3+} UCNPs with the particle sizes of 9.5 ± 0.9 nm and 11.0 ± 1.1 nm were obtained, respectively (Figs. 4(e)–4(g)). As the reaction time was prolonged, the particle sizes increased with the dissolution of the small particles and the re-deposition of the dissolved species on the surfaces of larger crystals, indicating that the formation and growth of hexagonal phase $NaYF_4$:Yb^{3+}/Er^{3+} UCNPs underwent an Ostwald ripening process [46]. In order to prepare pure hexagonal phase $NaYF_4$:Yb^{3+}/Er^{3+} UCNPs with small sizes and strong UC emission, the UCNPs treated at 310 ℃ for 30 min (Fig. 4(e)) were chosen as the precursors for later Gd^{3+}-exchange. After the addition of different doses of Gd^{3+}–oleate,

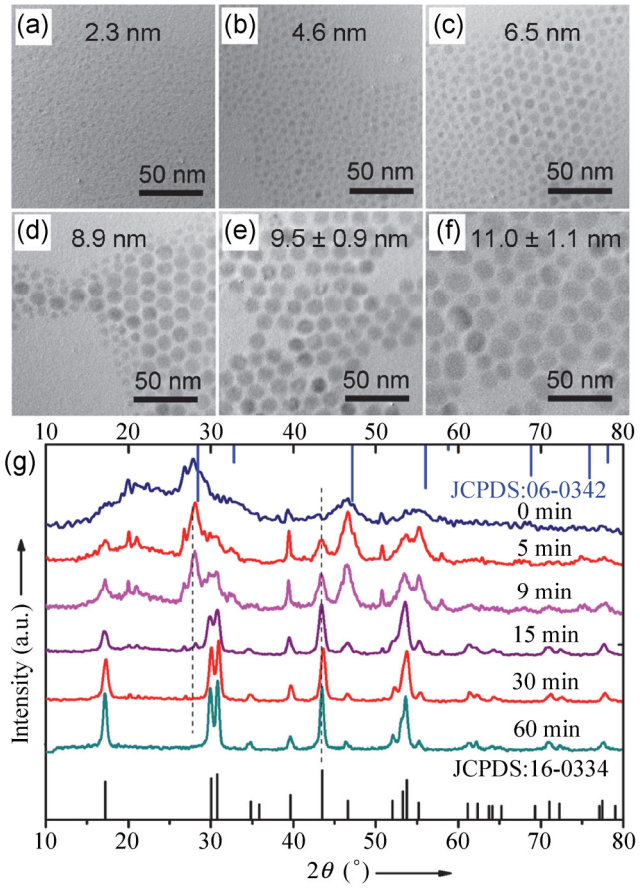

Figure 4 TEM images (a)–(f) and XRD patterns (g) of $NaYF_4$:Yb^{3+}/Er^{3+} UCNPs with different reaction time of 0 min (a), 5 min (b), 9 min (c), 15 min (d), 30 min (e), and 60 min (f). These UCNPs were prepared by controlling the reaction temperature at 310 ˚C. The $NaYF_4$ precursors were treated at relatively low temperature for a period of time before solvothermal treatment at 310 ˚C for 30 min (see the Section 2 for detail). Cubic phase (JCPDS: 06-0342); hexagonal phase (JCPDS: 16-0334).

the reaction system was treated at 310 ˚C for another 30 min and the total solvothermal time was 1 h for each Gd^{3+}-exchanged sample.

As mentioned above, we selected the β-$NaYF_4$:Yb/Er ($Y^{3+}/Yb^{3+}/Er^{3+}$ = 80/15/5) UCNPs with green UC luminescence to investigate the luminescence enhancement via Gd^{3+}–exchange. After Gd^{3+}-exchange, the green UC luminescence of the Gd^{3+}-exchanged β-$NaYF_4$:Yb/Er ($Y^{3+}/Yb^{3+}/Er^{3+}$ = 80/15/5) UCNPs was enhanced 29 times relative to that of the β-$NaYF_4$:Yb/Er UCNPs even though the total solvothermal time (at 310 ˚C) was identical (60 min) for both cases, with and without Gd^{3+}-exchange. Meanwhile, the particle sizes of the UCNPs have no obvious change after the Gd^{3+}-exchange. These results suggest that Gd^{3+}-exchange is a very useful strategy to greatly enhance the UC luminescence while maintaining the small particle size. To further investigate Gd^{3+}-exchange on the surface of nanocrystals, $NaYF_4$:Yb^{3+}/Er^{3+} NRs were also prepared by increasing the amount of oleic acid in the preparation of nanocrystals (Fig. S4 in the ESM). The Gd^{3+}-exchanged NRs were prepared via solvothermal treatment of $NaYF_4$:Yb^{3+}/Er^{3+} NRs seeds (length/diameter = ~46/~26 nm) (Fig. S4(a) in the ESM and Fig. 5(a)) with different amounts of Gd^{3+}–oleate. Compared with the shape and size of $NaYF_4$ NRs seeds (Figs. 5(a1)–5(a3)), after the Gd^{3+}-exchange, the shape rather than the size of the NRs showed some change (Figs. 5(b) and 5(c)). The HRTEM images

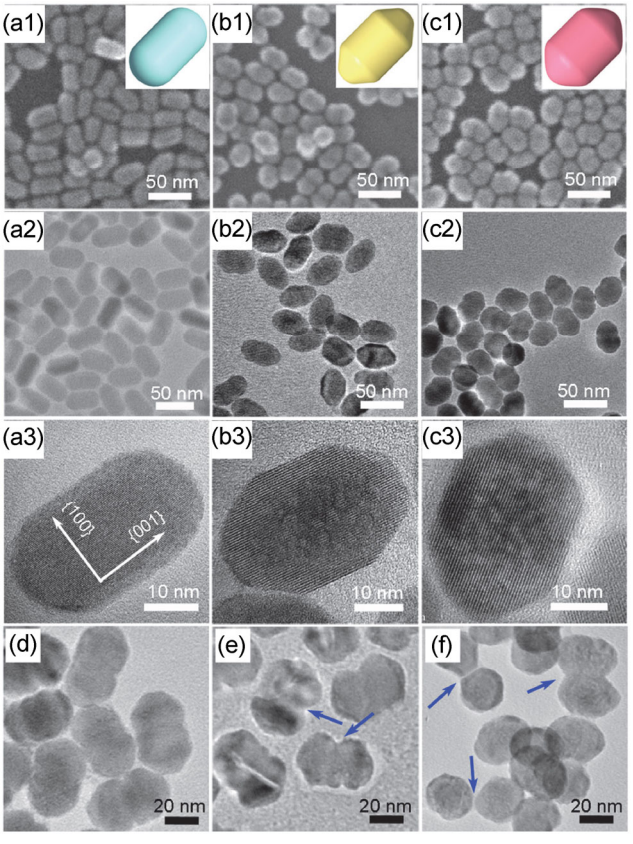

Figure 5 SEM (a1)–(c1), TEM (a2)–(c2) and HRTEM (a3)–(c3) images of $NaYF_4$:Yb^{3+}/Er^{3+} NRs prepared by exchanging with 0 mmol (a), 0.25 mmol (b), and 0.5 mmol (c) of Gd^{3+} in $NaYF_4$:Yb^{3+}/Er^{3+} rod seeds (1.0 mmol), respectively, and TEM images of Gd^{3+}(0.5mmol)-exchanged $NaYF_4$:Yb^{3+}/Er^{3+} NRs treated at 310 ˚C for (d) 0.5 h, (e) 1.0 h, and (f) 1.5 h. The Gd^{3+}–oleate was injected after the formation of $NaYF_4$:Yb^{3+}/Er^{3+} NRs (1 h, 310 ˚C) and then treated at 310 ºC for another 0.5 h (a)–(d), 1.0 h (e) and 1.5 h (f).

indicated that the Gd^{3+}–exchange was mainly carried out along the short axis direction {100} while the long axis {001} underwent some shrinking instead (Figs. 5(b) and 5(c)). When 0.25 mmol (Fig. 5(b)) or 0.5 mmol (Fig. 5(c)) of Gd^{3+}–oleate was used, the diameter of the as-prepared NRs increased to ~29 and ~31 nm while the length decreased to ~44 and ~43 nm, respectively. The influence of the reaction time on the NRs shape after the addition of Gd^{3+} (0.5 mmol) was also assessed by prolonging the reaction time (Figs. 5(d)–5(f)). As the Gd^{3+}–treated NRs solution was heated at 310 ˚C for 1 h, obvious shrinkage defects appeared near the centre of the rod side (Fig. 5(e)) and the NRs were finally bisected into two particles and aggregated when the reaction time was prolonged to 1.5 h (Fig. 5(f)). As we demonstrated in our previous work, excess F-precursor is highly desirable for the formation of $NaYF_4$ nanorods [36, 37, 62], where the crystal growth is along the (001) lattice plane due to its high surface energy. However, in the current work, when the Gd^{3+}-precursor was added, the F-precursor is deficient, and thus the surface energy of the (100) lattice plane is higher than that of the (001) face, which results in the Gd^{3+}-exchange on this face. As a result, the nanorods were broken into two nanoparticles. These results further suggest that the $NaGdF_4$ formation is through Gd^{3+}-exchange instead of shell coating.

To demonstrate the bioapplications of these Gd^{3+}-exchanged $NaYF_4$ NPs, modified amphiphilic poly(amino acid) was used to encapsulate these hydrophobic NPs with one particle per micelle and the cytotoxicity of the hydrophilic NPs toward the HepG2 cancer cell was investigated by means of methyl thiazolyl tetrazolium (MTT) assay. After the poly(amino acid) coating, the average hydrodynamic size of the NPs increased to ~20.7 nm from ~17.2 nm (Fig. S5 in the ESM). The TEM image (Fig. 6(a)) and the hydrodynamic diameter distribution of the hydrophilic NPs indicated the hydrophobic UCNPs were successfully encapsulated into the poly(amino acid) with one particle per micelle and no aggregation was found. As shown in UC luminescence spectra (Fig. S5(c)), compared to the luminescence of the hydrophobic nanoparticles before surface functionalization, about 54% of the luminescence was quenched after the surface modification. This can be attributed mainly to the high frequency vibration of the grafted poly(amino acid) after surface modification. The cytotoxicity of the hydrophilic NPs was also investigated in detail. As shown in Fig. 6(b), when the HepG2 cancer cells were incubated with 100 μg/mL of hydrophilic NPs for 24 h, more than 92% of cells survived. Even when the cells were incubated with 200 μg/mL of UCNPs for 48 h, about 83% cells remained alive. These results clearly indicate that the poly(amino acid) functionalized UCNPs display good biocompatibility.

Due to the novel advantages of UCNPs including NIR excitation with deep penetration, excellent luminescence stability, and low autofluorescence interference, the targeted UC luminescence imaging of

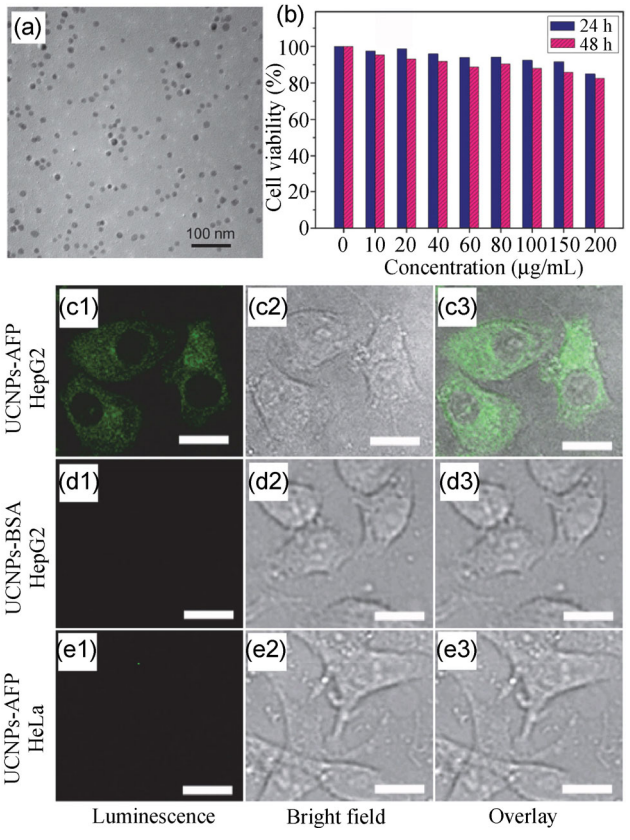

Figure 6 (a) TEM image of Gd^{3+}-exchanged UCNPs after functionalization with poly(amino acid) and dispersal in aqueous media. (b) Cell viability tests of hydrophilic UCNPs on HepG2 cancer cells incubated for 24 h (blue) and 48 hours (red). (c)–(e) Confocal UC luminescence imaging of HepG2 cells stained with UCNPs–Ab (anti-AFP) ((c1)–(c3)), HepG2 cells incubated with UCNPs without Ab (anti-AFP) modification ((d1)–(d3)), and HeLa cells incubated with UCNPs–Ab (anti-AFP) ((e1)–(e3)) for 4 h. Scale bars are 20 μm.

cancer cells with these UCNPs as probes was investigated via a TCS SP5 confocal microscope equipped with a NIR (980-nm) laser. These poly(amino acid) modified NPs were conjugated with anti-α-fetoprotein (anti-AFP) antibody (Ab). HepG2 cancer cells were then incubated with 100 μg/mL of UCNPs–Ab in 5% CO_2 at 37 ℃ for 4 h. After washing away the unbound nanocrystals, the cells were imaged using 980-nm irradiation. The UC emission at 543 ± 10 nm was used as the output signal of the collecting channel. Strong green UC luminescence of the UCNPs–Ab was observed clearly on the HepG2 cells (Fig. 6(c1)–6(c3)). In addition, large area luminescence imaging with more cells is shown in Fig. S6 (in the ESM). It is notable that the NPs are as well dispersed on the cell surface as the organic dyes, and no aggregation was found, suggesting a very good dispersibility in aqueous media after surface functionalization with poly(amino acid). Meanwhile, no green UC luminescence was detected from the HepG2 cells treated with the same concentration of NPs without Ab (Fig. 6 (d1)–6(d3)) or from the HeLa cells treated with the same concentration of NPs–Ab (Fig. 6(e1)–6(e3)), suggesting a very good targeted imaging ability of the Ab-bioconjugated UCNPs.

4 Conclusions

We have developed a facile one-pot *in situ* Gd^{3+}-exchange strategy to dramatically improve the luminescence of UCNPs while keep the particle size and shape unchanged. After Gd^{3+}-exchange, UC luminescence of the NPs was enhanced about 29 times whilst retaining the particle size and shape. To the best of our knowledge, this is the first report of greatly enhanced green UC emission of $NaYF_4$:Yb^{3+}/Er^{3+} NPs with retained small particle size (~11.8 nm) using a one-pot *in situ* Gd^{3+}-exchange strategy. The hydrophobic UCNPs were then successfully employed for targeted cell UC luminescence imaging after surface functionalization by grafting poly(amino acid) to afford the individual hydrophilic and biocompatible NPs. This study offers an efficient way to prepare highly luminescent NPs with small particle size and has great potential applications in nanobiotechnology due to the good biocompatibility, small particle size, and strong luminescence of the as-prepared nanocrystals.

Acknowledgements

This research was supported in part by the National Natural Science Foundation of China (Grant No. 21275015), the State Key Project of Fundamental Research of China (Grant Nos. 2011CBA00503 and 2011CB932403), the Program for New Century Excellent Talents in University of China (No. NCET100213), the Science Foundation of Xinjiang Uygur Autonomous Region (201191170), the Fundamental Research Funds for the Central Universities(ZZ1321), and the Scientific Research Foundation for the Returned Overseas Chinese Scholars, State Education Ministry.

Electronic Supplementary Material: Supplementary materials (XRD, energy dispersive X-ray spectroscopy, DLS size distribution measurements, TEM imaging and large-area cell imaging) is available in the online version of this article at http://dx.doi.org/10.1007/s12274-014-0439-6.

References

[1] Chen, G. Y.; Ohulchanskyy, T. Y.; Kumar, R.; Agren, H.; Prasad, P. N. Ultrasmall monodisperse $NaYF_4$:Yb^{3+}/Tm^{3+} nanocrystals with enhanced near-infrared to near-infrared upconversion photoluminescence. *ACS Nano* **2010**, *4*, 3163–3168.

[2] Xiong, L. Q.; Chen, Z. G.; Tian, Q. W.; Cao, T. Y.; Xu, C. J.; Li, F. Y. High contrast upconversion luminescence targeted imaging *in vivo* using peptide-labeled nanophosphors. *Anal. Chem.* **2009**, *81*, 8687–8694.

[3] Liu, Q.; Sun, Y.; Yang, T. S.; Feng, W.; Li, C. G.; Li, F. Y. Sub-10 nm hexagonal lanthanide-doped $NaLuF_4$ upconversion nanocrystals for sensitive bioimaging *in vivo*. *J. Am. Chem. Soc.* **2011**, *133*, 17122–17125.

[4] Zhang, C. M.; Lin, J. Defect-related luminescent materials: Synthesis, emission properties and applications. *Chem. Soc. Rev.* **2012**, *41*, 7938–7961.

[5] Wang, F.; Liu, X. G. Upconversion multicolor fine-tuning: Visible to near-infrared emission from lanthanide-doped $NaYF_4$ nanoparticles. *J. Am. Chem. Soc.* **2008**, *130*, 5642–5643.

[6] Wang, F.; Han, Y.; Lim, C. S.; Lu, Y. H.; Wang, J.; Xu, J.; Chen, H. Y.; Zhang, C.; Hong, M. H.; Liu, X. G. Simultaneous

phase and size control of upconversion nanocrystals through lanthanide doping. *Nature* **2010**, *463*, 1061–1065.

[7] Wang, F.; Wang, J. A.; Liu, X. G. Direct evidence of a surface quenching effect on size-dependent luminescence of upconversion nanoparticles. *Angew. Chem.–Int. Edit.* **2010**, *49*, 7456–7460.

[8] Liu, Q.; Peng, J. J.; Sun, L. N.; Li, F. Y. High-efficiency upconversion luminescent sensing and bioimaging of Hg(II) by chromophoric ruthenium complex-assembled nanophosphors. *ACS Nano* **2011**, *5*, 8040–8048.

[9] Xia, A.; Gao, Y.; Zhou, J.; Li, C. Y.; Yang, T. S.; Wu, D. M.; Wu, L. M.; Li, F. Y. Core–shell $NaYF_4$:Yb^{3+},Tm^{3+}@Fe_xO_y nanocrystals for dual-modality T_2-enhanced magnetic resonance and NIR-to-NIR upconversion luminescent imaging of small-animal lymphatic node. *Biomaterials* **2011**, *32*, 7200–7208.

[10] Zhou, J.; Yu, M. X.; Sun, Y.; Zhang, X. Z.; Zhu, X. J.; Wu, Z. H.; Wu, D. M.; Li, F. Y. Fluorine-18-labeled Gd^{3+}/Yb^{3+}/Er^{3+} co-doped $NaYF_4$ nanophosphors for multimodality PET/MR/UCL imaging. *Biomaterials* **2011**, *32*, 1148–1156.

[11] Zhou, J.; Liu, Z.; Li, F. Y. Upconversion nanophosphors for small-animal imaging. *Chem. Soc. Rev.* **2012**, *41*, 1323–1349.

[12] Jiang, S.; Zhang, Y. Upconversion nanoparticle-based FRET system for study of siRNA in live cells. *Langmuir* **2010**, *26*, 6689–6694.

[13] Deng, M. L.; Tu, N.; Bai, F.; Wang, L. Y. Surface functionalization of hydrophobic nanocrystals with one particle per micelle for bioapplications. *Chem. Mater.* **2012**, *24*, 2592–2597.

[14] Wang, F.; Banerjee, D.; Liu, Y. S.; Chen, X. Y.; Liu, X. G. Upconversion nanoparticles in biological labeling, imaging, and therapy. *Analyst* **2010**, *135*, 1839–1854.

[15] Cheng, L. A.; Yang, K.; Zhang, S. A.; Shao, M. W.; Lee, S. T.; Liu, Z. Highly-sensitive multiplexed in vivo imaging using PEGylated upconversion nanoparticles. *Nano Res.* **2010**, *3*, 722–732.

[16] Yang, Y. M.; Shao, Q.; Deng, R. R.; Wang, C.; Teng, X.; Cheng, K.; Cheng, Z.; Huang, L.; Liu, Z.; Liu, X. G. et al.. In vitro and in vivo uncaging and bioluminescence imaging by using photocaged upconversion nanoparticles. *Angew. Chem. Int. Edit.* **2012**, *51*, 3125–3129.

[17] Wang, L. Y.; Li, Y. D. Green upconversion nanocrystals for DNA detection. *Chem. Commun.* **2006**, 2557–2559.

[18] Wang, C.; Tao, H. Q.; Cheng, L.; Liu, Z. Near-infrared light induced *in vivo* photodynamic therapy of cancer based on upconversion nanoparticles. *Biomaterials* **2011**, *32*, 6145–6154.

[19] Ang, L. Y.; Lim, M. E.; Ong, L. C.; Zhang, Y. Applications of upconversion nanoparticles in imaging, detection and therapy. *Nanomedicine* **2011**, *6*, 1273–1288.

[20] Dai, Y. L.; Yang, D. M.; Ma, P. A.; Kang, X. J.; Zhang, X.; Li, C. X.; Hou, Z. Y.; Cheng, Z. Y.; Lin, J. Doxorubicin conjugated $NaYF_4$:Yb^{3+}/Tm^{3+} nanoparticles for therapy and sensing of drug delivery by luminescence resonance energy transfer. *Biomaterials* **2012**, *33*, 8704–8713.

[21] Yang, D. M.; Li, G. G.; Kang, X. J.; Cheng, Z. Y.; Ma, P. A.; Peng, C.; Lian, H. Z.; Li, C. X.; Lin, J. Room temperature synthesis of hydrophilic Ln^{3+}-doped $KGdF_4$ (Ln = Ce, Eu, Tb, Dy) nanoparticles with controllable size: Energy transfer, size-dependent and color-tunable luminescence properties. *Nanoscale* **2012**, *4*, 3450–3459.

[22] Deng, M. L.; Ma, Y. X.; Huang, S.; Hu, G. F.; Wang, L. Y. Monodisperse upconversion $NaYF_4$ nanocrystals: Syntheses and bioapplications. *Nano Res.* **2011,** *4*, 685–694.

[23] Li, H.; Wang, L. Y. $NaYF_4$:Yb^{3+}/Er^{3+} nanoparticle-based upconversion luminescence resonance energy transfer sensor for mercury(II) quantification. *Analyst* **2013**, *138*, 1589–1595.

[24] An, M. Y.; Cui, J. B.; He, Q.; Wang, L. Y. Down-/up-conversion luminescence nanocomposites for dual-modal cell imaging. *J. Mater. Chem. B* **2013**, *1*, 1333–1339.

[25] Li, H.; Wang, L. Y. Preparation and upconversion luminescence cell imaging of O-carboxymethyl chitosan-functionalized $NaYF_4$:Yb^{3+}/Tm^{3+}/Er^{3+} nanoparticles. *Chin. Sci. Bull.* **2013**, *58*, 4051–4056.

[26] Shan, J. N.; Uddi, M.; Yao, N.; Ju, Y. G. Anomalous Raman scattering of colloidal Yb^{3+},Er^{3+} codoped $NaYF_4$ nanophosphors and dynamic probing of the upconversion luminescence. *Adv. Funct. Mater.* **2010**, *20*, 3530–3537.

[27] Wang, L. Y.; Yan, R. X.; Hao, Z. Y.; Wang, L.; Zeng, J. H.; Bao, H.; Wang, X.; Peng, Q.; Li, Y. D. Fluorescence resonant energy transfer biosensor based on upconversion-luminescent nanoparticles. *Angew. Chem. Int. Edit.* **2005**, *44*, 6054–6057.

[28] Yin, A. X.; Zhang, Y. W.; Sun, L. D.; Yan, C. H. Colloidal synthesis and blue based multicolor upconversion emissions of size and composition controlled monodisperse hexagonal $NaYF_4$:Yb,Tm nanocrystals. *Nanoscale* **2010**, *2*, 953–959.

[29] Wang, Y. H.; Cai, R. X.; Liu, Z. H. Controlled synthesis of $NaYF_4$:Yb,Er nanocrystals with upconversion fluorescence via a facile hydrothermal procedure in aqueous solution. *CrystEngComm* **2011**, *13*, 1772–1774.

[30] Zhang, H.; Li, Y. J.; Lin, Y. C.; Huang, Y.; Duan, X. F. Composition tuning the upconversion emission in $NaYF_4$: Yb/Tm hexaplate nanocrystals. *Nanoscale* **2011**, *3*, 963–966.

[31] Li, Z. Q.; Zhang, Y. An efficient and user-friendly method for the synthesis of hexagonal-phase $NaYF_4$: Yb, Er/Tm nanocrystals with controllable shape and upconversion fluorescence. *Nanotechnology* **2008**, *19*, 345606.

[32] Zhang, H.; Li, Y. J.; Ivanov, I. A.; Qu, Y. Q.; Huang, Y.; Duan, X. F. Plasmonic modulation of the upconversion fluorescence in $NaYF_4$:Yb/Tm hexaplate nanocrystals using gold nanoparticles or nanoshells. *Angew. Chem. Int. Edit.* **2010**, *49*, 2865–2868.

[33] Zhang, H.; Xu, D.; Huang, Y.; Duan, X. F. Highly spectral dependent enhancement of upconversion emission with sputtered gold island films. *Chem. Commun.* **2011**, *47*, 979–981.

[34] Mai, H. X.; Zhang, Y. W.; Sun, L. D.; Yan, C. H. Highly efficient multicolor up-conversion emissions and their mechanisms of monodisperse $NaYF_4$:Yb,Er core and core/shell-structured nanocrystals. *J. Phys. Chem. C* **2007**, *111*, 13721–13729.

[35] Liang, X.; Wang, X.; Zhuang, J.; Peng, Q.; Li, Y. D. Synthesis of $NaYF_4$ nanocrystals with predictable phase and shape. *Adv. Funct. Mater.* **2007**, *17*, 2757–2765.

[36] Wang, L. Y.; Li, Y. D. Controlled synthesis and luminescence of lanthanide doped $NaYF_4$ nanocrystals. *Chem. Mater.* **2007**, *19*, 727–734.

[37] Wang, L. Y.; Li, Y. D. $Na(Y_{1.5}Na_{0.5})F_6$ single-crystal nanorods as multicolor luminescent materials. *Nano Lett.* **2006**, *6*, 1645–1649.

[38] Liu, Y. X.; Wang, D. S.; Shi, J. X.; Peng, Q.; Li, Y. D. Magnetic tuning of upconversion luminescence in lanthanide-doped bifunctional nanocrystals. *Angew. Chem. Int. Edit.* **2013**, *52*, 4366–4369.

[39] Li, H.; Wang, L. Y. Controllable multicolor upconversion luminescence by tuning the NaF dosage. *Chem.—Asian J.* **2014**, *9*, 153–157.

[40] Bednarkiewicz, A.; Wawrzynczyk, D.; Gagor, A.; Kepinski, L.; Kurnatowska, M.; Krajczyk, L.; Nyk, M.; Samoc, M.; Strek, W. Giant enhancement of upconversion in ultra-small Er^{3+}/Yb^{3+}:$NaYF_4$ nanoparticles via laser annealing. *Nanotechnology* **2012**, *23*, 145705.

[41] Wang, H. Q.; Nann, T. Monodisperse upconverting nanocrystals by microwave-assisted synthesis. *ACS Nano* **2009**, *3*, 3804–3808.

[42] Abel, K. A.; Boyer, J. C.; Andrei, C. M.; van Veggel, F. Analysis of the shell thickness distribution on $NaYF_4$/$NaGdF_4$ core/shell nanocrystals by EELS and EDS. *J. Phys. Chem. Lett.* **2011**, *2*, 185–189.

[43] Guo, H.; Li, Z. Q.; Qian, H. S.; Hu, Y.; Muhammad, I. N. Seed-mediated synthesis of $NaYF_4$:Yb, Er/$NaGdF_4$ nanocrystals with improved upconversion fluorescence and MR relaxivity. *Nanotechnology* **2010**, *21*, 125602.

[44] Wang, X.; Zhuang, J.; Peng, Q.; Li, Y. D. A general strategy for nanocrystal synthesis. *Nature* **2005**, *437*, 121–124.

[45] Liang, X.; Wang, X.; Zhuang, J.; Peng, Q.; Li, Y. D. Branched $NaYF_4$ nanocrystals with luminescent properties. *Inorg. Chem.* **2007**, *46*, 6050–6055.

[46] Mai, H. X.; Zhang, Y. W.; Si, R.; Yan, Z. G.; Sun, L. D.; You, L. P.; Yan, C. H. High-quality sodium rare-earth fluoride nanocrystals: Controlled synthesis and optical properties. *J. Am. Chem. Soc.* **2006**, *128*, 6426–6436.

[47] Vetrone, F.; Naccache, R.; Mahalingam, V.; Morgan, C. G.; Capobianco, J. A. The active-core/active-shell approach: A strategy to enhance the upconversion luminescence in lanthanide-doped nanoparticles. *Adv. Funct. Mater.* **2009**, *19*, 2924–2929.

[48] Boyer, J. C.; Manseau, M. P.; Murray, J. I.; van Veggel, F. Surface modification of upconverting $NaYF_4$ nanoparticles with PEG-phosphate ligands for NIR (800 nm) biolabeling within the biological window. *Langmuir* **2010**, *26*, 1157–1164.

[49] Song, C. H.; Ye, Z. Q.; Wang, G. L.; Yuan, J. L.; Guan, Y. F. Core-shell nanoarchitectures: A strategy to improve the efficiency of luminescence resonance energy transfer. *ACS Nano* **2010**, *4*, 5389–5397.

[50] Chaudhuri, R. G.; Paria, S. Core/shell nanoparticles: Classes, properties, synthesis mechanisms, characterization, and applications. *Chem. Rev.* **2012**, *112*, 2373–2433.

[51] Wang, Y.; Tu, L. P.; Zhao, J. W.; Sun, Y. J.; Kong, X. G.; Zhang, H. Upconversion luminescence of β-$NaYF_4$:Yb^{3+}, Er^{3+}@β-$NaYF_4$ core/shell nanoparticles: Excitation power, density and surface dependence. *J. Phys. Chem. C* **2009**, *113*, 7164–7169.

[52] Schafer, H.; Ptacek, P.; Zerzouf, O.; Haase, M. Synthesis and optical properties of KYF_4/Yb,Er nanocrystals, and their surface modification with undoped KYF_4. *Adv. Funct. Mater.* **2008**, *18*, 2913–2918.

[53] Yi, G. S.; Chow, G. M. Water-soluble $NaYF_4$:Yb,Er(Tm)/$NaYF_4$/polymer core/shell/shell nanoparticles with significant enhancement of upconversion fluorescence. *Chem. Mater.* **2007**, *19*, 341–343.

[54] Zhang, C.; Lee, J. Y. Prevalence of anisotropic shell growth in rare earth core–shell upconversion nanocrystals. *ACS Nano* **2013**, *7*, 4393–4402.

[55] Su, Q. Q.; Han, S. Y.; Xie, X. J.; Zhu, H. M.; Chen, H. Y.; Chen, C. K.; Liu, R. S.; Chen, X. Y.; Wang, F.; Liu, X. G. The effect of surface coating on energy migration-mediated upconversion. *J. Am. Chem. Soc.* **2012**, *134*, 20849–20857.

[56] Qian, H. S.; Zhang, Y. Synthesis of hexagonal-phase core-shell $NaYF_4$ nanocrystals with tunable upconversion fluorescence. *Langmuir* **2008**, *24*, 12123–12125.

[57] Son, D. H.; Hughes, S. M.; Yin, Y. D.; Alivisatos, A. P. Cation exchange reactions in ionic nanocrystals. *Science* **2004**, *306*, 1009–1012.

[58] Abel, K. A.; Qiao, H. J.; Young, J. F.; van Veggel, F. Four-fold enhancement of the activation energy for nonradiative decay of excitons in PbSe/CdSe core/shell versus PbSe colloidal quantum dots. *J. Phys. Chem. Lett.* **2010**, *1*, 2334–2338.

[59] Dong, C. H.; Korinek, A.; Blasiak, B.; Tomanek, B.; van Veggel, F. Cation exchange: A facile method to make $NaYF_4$:Yb,Tm–$NaGdF_4$ core–shell nanoparticles with a thin, tunable, and uniform shell. *Chem. Mater.* **2012**, *24*, 1297–1305.

[60] Huang, S.; Bai, M.; Wang, L. Y. General and facile surface functionalization of hydrophobic nanocrystals with poly(amino acid) for cell luminescence imaging *Sci. Rep.* **2013**, *3*, 2023.

[61] Tu, N. N.; Wang, L. Y. Surface plasmon resonance enhanced upconversion luminescence in aqueous media for TNT selective detection. *Chem. Commun.* **2013**, *49*, 6319–6321.

[62] Wang, L. Y.; Li, P.; Li, Y. D. Down- and up-conversion luminescent nanorods. *Adv. Mater.* **2007**, *19*, 3304–3307.

[63] Feng, W.; Sun, L. D.; Zhang, Y. W.; Yan, C. H. Solid-to-hollow single-particle manipulation of a self-assembled luminescent $NaYF_4$:Yb,Er nanocrystal monolayer by electron-beam lithography. *Small* **2009**, *5*, 2057–2060.

[64] Wei, Y.; Lu, F. Q.; Zhang, X. R.; Chen, D. P. Synthesis of oil-dispersible hexagonal-phase and hexagonal-shaped $NaYF_4$:Yb,Er nanoplates. *Chem. Mater.* **2006**, *18*, 5733–5737.